Optical Modeling for Dynamics and Control Analysis

David C. Redding*
Charles Stark Draper Laboratory, Cambridge, Massachusetts 02139
and
William G. Breckenridge†
Jet Propulsion Laboratory, California Institute of Technology, Pasadena, California 91109

This paper presents a coordinate-free ray-trace analysis of optical beam trains consisting of mirrors, lenses, and reference surfaces. The analysis leads to optical models that can be directly integrated with standard structure and control models for integrated instrument design, analysis, and simulation. This capability is required for a coming generation of space-borne optical instruments that use controlled optical elements supported by flexible structures. New results include analytic formulas for optical sensitivities as functions of structural and control geometric parameters. An example problem calculates a linear (small-motion) optical model, derives optical gains for small- and large-angle controlled mirrors, and shows the propagation of a wave front.

Nomenclature

a = ellipse semimajor axis length
$d\hat{i}$ = small deviation from the nominal $\hat{i}$; $d\hat{i}$ is perpendicular to $\hat{i}$
$d\hat{r}$ = small deviation from the nominal $\hat{r}$; $d\hat{r}$ is perpendicular to $\hat{r}$
dL = optical path-length difference from nominal; the perturbation in path length along the incident ray
e = eccentricity of a conic section
f = distance from vertex to focus of a conic section
I = identity dyad (or matrix)
$\hat{i}$ = incident ray direction
L_i = vector from the incident ray reference point to the reflection (or refraction) point
M = surface dyadic for an element
N = vector in the normal direction at ρ with magnitude equal to the element radius of curvature at ρ
$\hat{N}$ = unit normal vector out of the surface opposite to the incident ray
n = index of refraction
P_u = projection dyadic, $= I - \hat{u}\hat{u}$; $P_u v$ is the part of v perpendicular to $\hat{u}$
p = semilatus rectum of a conic section; also the magnitude of p
p = reference point for incident ray
q = vector from the element vertex to the element rotation point
R = reflection dyadic, $\hat{R} = I - 2\hat{N}\hat{N}$
$\hat{r}$ = reflected (or refracted) ray direction
u_i = ray perturbation state at the ith element, $\equiv \begin{bmatrix} \hat{\theta}_i \\ \delta_i \end{bmatrix}$
v = magnitude of v
$\hat{v}$ = unit vector in direction of v
$v^\times$ = cross-product matrix operator, $= \begin{bmatrix} 0 & -v_z & v_y \\ v_z & 0 & -v_x \\ -v_y & v_x & 0 \end{bmatrix}$
$\tilde{v}$ = cross-dyadic $\tilde{v}$
x_i = ray perturbation state at the ith element, $\equiv \begin{bmatrix} d\hat{r}_i \\ \gamma_i \\ dL_i \end{bmatrix}$
α = incident-ray transverse aberration (beamwalk), measured at the incident ray reference point; α is perpendicular to $\hat{i}$
β = beamwalk at the input of the element; β is perpendicular to $\hat{i}$
γ = reflected-ray transverse aberration (beamwalk) from the nominal ray position, measured at the nominal output of the element; γ is perpendicular to $\hat{r}$
δ = small translational deflection of the element
θ = small angular deflection (tilt) of the element about a specified point
ρ = vector from the element vertex to the point of incidence of a ray on the element surface
$\hat{\Psi}$ = principal axis vector of an element taken from the vertex toward the focus
$\frac{\partial x_i}{\partial x_{i-1}}$ = transition matrix from the $i-1$ to the ith element
$\frac{\partial x_i}{\partial u_i}$ = influence matrix at the ith element

Subscript
i = ith element in an optical beam train

Received Dec. 8, 1989; revision received July 6, 1990; accepted for publication Aug. 2, 1990; presented as Paper 90-3383 at the AIAA Guidance, Navigation, and Control Conference, Portland, OR, Aug. 20-22, 1990.

*Site Manager, JPL 185, 4800 Oak Grove Drive, Pasadena, CA 91109. Member AIAA.
†Section Staff, JPL 185, 4800 Oak Grove Drive.

I. Introduction

OPTICAL instruments typically collect, guide, and process beams of light using a sequence of optical elements such as mirrors and lenses. The light may be compressed or expanded, focused on a image plane, combined with other beams at a pupil, or transmitted to a distant target, depending on the instrument's function. Performance of the instrument depends on the optical elements maintaining their nominal

alignment and figure. Deviations from the nominal beam train geometry due to deformations of the instrument structure or to controller actions can move the instrument line of sight, distort images, lower signal-to-noise ratios, reduce the crispness of interference fringes, or decrease the quality of an outgoing wave front. For large space-borne optical instruments, especially, these effects can be critical and must be modeled to permit the design of optical pointing controllers, wave-front controllers, and active structure controllers, to perform instrument error analysis and calibration, and to analyze and simulate end-to-end instrument performance. These instruments include long-baseline optical interferometers, large telescopes using multisegmented reflectors, and laser-beam relay optics for communications or power delivery purposes.[1-5]

To date, the design and analysis of such instruments has been necessarily piecemeal, with little opportunity to conduct design tradeoffs that cross disciplinary boundaries. Existing optical modeling computer tools have been used to provide point-design models that are valid only for small motions of the instrument. These models are computed by numerical differentiation or other approximate methods. The derivation of optical models and optical sensitivities that are valid over large motions, required for controller design, has required specialized analysis and has not accounted for wave-front phase effects.[6,7]

This paper presents the mathematics underlying a new, more versatile approach to modeling optics. Our approach is based on geometric ray-trace optics; diffraction effects have also been incorporated but are not discussed here. It uses a powerful coordinate-free notation and modular optical element representation to provide generality. Analytical formulas are derived for exact optical sensitivities. Our approach systematizes the creation of small- and large-motion optical models that are functions of structure and control as well as optical parameters. Realized in computer code, it offers the tools necessary for conducting truly integrated optical instrument design and analysis, providing accurate optical models that are directly integrable with standard structure and control models. It enables rapid cross-disciplinary design trade studies, even automated integrated structures/optics/control design optimization.[8]

The discussion in this paper starts with the law of reflection of light, deriving coordinate-free expressions for tracing a ray past a mirror. Perturbations of the incident ray and the mirror position and attitude are then considered, and the sensitivities of the reflected ray to these perturbations are derived. Refracting surfaces are analyzed, developing a coordinate-free form of Snell's law and deriving the sensitivities of a refracted ray. Next, we examine multiple-surface beam trains. Rays are traced through a beam train by successive application of the exact reflection and refraction ray-trace equations developed in the earlier sections. Adopting matrix notation in the structural coordinate frame, optical sensitivities are used as transition matrices in a difference equation that propagates the perturbation ray state from element to element. The transition matrices are combined to create linear models of the optics in structural coordinates. We then show how to incorporate control system sensor and actuator coordinates directly into the optical models.

An interferometer beam-compressor telescope provides an example of the application of our approach. We compute a line-of-sight optical model and use it to show sensitivities to element alignment error and to compute optical gains for a small-motion fast-steering mirror and a large-motion siderostat mirror. We show a wave-front phase plot and a spot diagram for a particular set of disturbances.

II. Effect of a Mirror on an Incident Ray

The direction of a ray $\hat{r}$ reflected by the surface of a mirror is dependent on the direction of the mirror normal $\hat{N}$ at the point where the incident ray $\hat{i}$ strikes the mirror. The mirror normal is in turn a function of mirror shape, position, and attitude and of the incident ray position and direction. In this section, we show how a particular mirror normal is determined for a particular incident ray. We derive incident ray path length and direction and reflected ray direction to provide a complete description of the ray through the mirror.

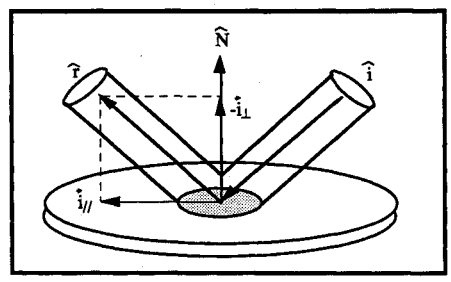

Fig. 1 Mirror reflection geometry.

The law of reflection states that the effect of a mirror on a ray $\hat{i}$ incident upon it is to reverse the normal component of $\hat{i}$, while leaving the parallel components of $\hat{i}$ unchanged (Fig. 1). The normal component of $\hat{i}$ is the component parallel to the mirror normal $\hat{N}$:

$$i_\perp = (\hat{N}\cdot\hat{i})\hat{N} = \hat{N}\hat{N}\cdot\hat{i} \tag{1}$$

The component parallel to the surface is the component perpendicular to $\hat{N}$

$$i_{//} = \hat{i} - \hat{N}\hat{N}\cdot\hat{i} = P_N\cdot\hat{i} \tag{2}$$

Here, P_N is the projection dyadic of $\hat{N}$, so that $P_N\cdot\hat{i}$ is the projection (the in-plane component) of $\hat{i}$ onto the surface perpendicular to $\hat{N}$. The reflected beam $\hat{r}$ is the difference of $i_{//}$ and $i_\perp$,

$$\hat{r} = i_{//} - i_\perp = (I - 2\hat{N}\hat{N})\hat{i} \tag{3}$$

Equation (3) can be written in terms of the reflection dyadic R as

$$\hat{r} = R\cdot\hat{i} \tag{4}$$

where R is defined as

$$R = I - 2\hat{N}\hat{N} \tag{5}$$

This dyadic form of the law of reflection apparently first appeared in Ref. 10.

It is worth noting some of the properties of the projection and reflection dyadics. Both are independent of the sign of $\hat{N}$:

$$P_N = P_{-N} \tag{6}$$

$$R_N = R_{-N} \tag{7}$$

The projection dyadic can also be written in terms of the cross dyadic:

$$P_N = -\hat{N}^\times\cdot\hat{N}^\times \tag{8}$$

The dot product of P with itself is P:

$$P\cdot P\cdot\cdots\cdot P = P \tag{9}$$

Properties of R include

$$[R\cdot v]^\times = -R\cdot v^\times\cdot R \tag{10}$$

$$R\cdot R = I \tag{11}$$

In combination with P,

$$P \cdot R = R \cdot P = P \tag{12}$$

$$R + I = 2P \tag{13}$$

Most optical elements used in high-precision optical systems have nominally flat or conic-section-of-revolution surface shapes. These surfaces can be represented using the mirror principal-axis direction $\hat{\Psi}$ and two of the four conic-section parameters: the semimajor axis length a, the eccentricity e, the vertex-to-focus length f, and the semilatus rectum p. These quantities are related as

$$p = f(1+e) = a(1-e^2) \tag{14}$$

The four main types of conic-of-revolution surfaces are the spheroid, for which eccentricity $e=0$; the ellipsoid, with $0<e<1$; the paraboloid, with $e=1$; and the hyperboloid, with $e>1$. Flat mirrors present a degenerate subcase, with $e=0$ and $f=\infty$.

Each of these surfaces can be described in terms of a surface dyadic M as

$$M \equiv (I - e^2 \hat{\Psi}\hat{\Psi}) \tag{15}$$

The principal axis $\hat{\Psi}$ is defined as pointing from the mirror vertex toward the focus. Writing ρ for the vector from the mirror vertex to an arbitrary point on the surface of the mirror, the mirror surface is defined by

$$\rho \cdot M \cdot \rho + 2N_0 \cdot \rho = 0 \tag{16}$$

N_0 is the vector N, with direction along the surface normal and magnitude equal to the radius of curvature, evaluated at the mirror vertex:

$$N_0 = -p\hat{\Psi} \tag{17}$$

The vector N at an arbitrary point ρ on the surface is

$$N = N_0 + M\rho \tag{18}$$

The mirror normal unit vector $\hat{N}$ at ρ is parallel to N. We adopt a convention that $\hat{N}$ is pointed away from $\hat{\imath}$ (the direction of $\hat{N}$ is significant only for refractive elements):

$$\hat{N} = -\text{sign}(\hat{\imath} \cdot N)\frac{N}{N} \tag{19}$$

where the magnitude N (the radius of curvature at ρ) is

$$N = |N| \tag{20}$$

For flat mirrors, we adopt a convention that $e=0, f=\infty$, and $\hat{N} = N = \hat{\Psi}$.

The curvature of the mirror surface at ρ can be expressed as the spatial gradient of the normal, $\partial\hat{N}/\partial\rho$. Differentiating,

$$\frac{d\hat{N}}{d\rho} = -\text{sign}(\hat{\imath} \cdot N)\left[\frac{1}{N} I - \frac{\hat{N}}{N^2}(\rho \cdot M + N_0)\right] \cdot M$$

$$= -\text{sign}(\hat{\imath} \cdot N)\frac{1}{N} P_N \cdot M \tag{21}$$

Consider a ray with direction $\hat{\imath}$ originating at a point p with respect to the vertex of a mirror. ρ is the reflection point (the intersection of the ray with the surface of the mirror):

$$\rho = p + L\hat{\imath} \tag{22}$$

where L is the length of the incident ray. Substituting for ρ in Eq. (16), L is a solution of

$$(\hat{\imath} \cdot M \cdot \hat{\imath})L^2 + 2\hat{\imath} \cdot (M \cdot p + N_0)L + p \cdot (M \cdot p + 2N_0) = 0 \tag{23}$$

Note that the physical length L is not always the actual length traveled by a light ray. To represent the effect of rays in different media, the path length L is scaled by the index of refraction n of the medium:

$$L_{\text{scaled}} = nL \tag{24}$$

This is important when discussing refracting surfaces (Sec. V).

At this point, we have a complete and exact description of the ray reflected by the mirror. It starts at the specified point p with a direction $\hat{\imath}$. It travels a length L, determined by solving Eq. (23), hitting the surface of the mirror at the point ρ [Eq. (22)]. The normal $\hat{N}$ and reflection dyadic R at this point are calculated from Eqs. (19) and (5); the ray is reflected with direction $\hat{r} = R \cdot \hat{\imath}$.

To illustrate the application of these relations, we consider the example sketched in Fig. 2. The mirror shown is parabolic, with vertex-to-focus length f and eccentricity $e=1$. In the coordinate system centered at the vertex and oriented as shown, the mirror principal axis is

$$\hat{\Psi} = \begin{bmatrix} 0 \\ 1 \\ 0 \end{bmatrix} \tag{25}$$

so that

$$M = \begin{bmatrix} 1 & 0 & 0 \\ 0 & 0 & 0 \\ 0 & 0 & 1 \end{bmatrix} \tag{26}$$

$$N_0 = \begin{bmatrix} 0 \\ -2f \\ 0 \end{bmatrix} \tag{27}$$

The example incident ray originates at a point p

$$p = \begin{bmatrix} p_x \\ p_y \\ 0 \end{bmatrix} \tag{28}$$

and has direction

$$\hat{\imath} = \begin{bmatrix} 0 \\ -1 \\ 0 \end{bmatrix} \tag{29}$$

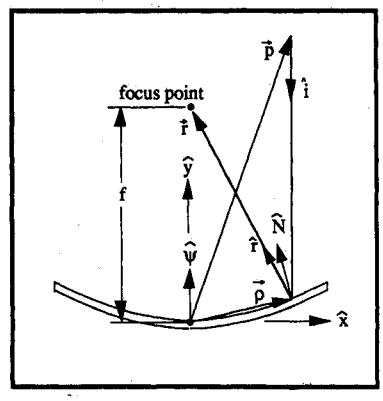

Fig. 2 Parabolic mirror example.

The ray length L is a root of Eq. (23). In this case, there is a unique root:

$$L = \frac{2fp_y - p_x^2}{4f} \tag{30}$$

The reflection point is

$$\rho = \begin{bmatrix} p_x \\ (2fp_y + p_x^2)/4f \\ 0 \end{bmatrix} \tag{31}$$

and the normal is

$$\hat{N} = \frac{1}{\sqrt{p_x^2 + 4f^2}} \begin{bmatrix} -p_x \\ 2f \\ 0 \end{bmatrix} \tag{32}$$

The reflected ray is determined from Eq. (4), where

$$R = \frac{1}{p_x^2 + 4f^2} \begin{bmatrix} -p_x^2 + 4f^2 & 4p_x f & 0 \\ 4p_x f & p_x^2 - 4f^2 & 0 \\ 0 & 0 & 1 \end{bmatrix} \tag{33}$$

The result is the reflected ray direction

$$\hat{r} = \frac{1}{p_x^2 + 4f^2} \begin{bmatrix} -4fp_x \\ 4f^2 - p_x^2 \\ 0 \end{bmatrix} \tag{34}$$

In this example, the incident ray is parallel to the parabolic mirror principal axis. Therefore, we expect that the reflected ray will pass through the mirror focus. Does it? The vector from the reflection point to the focus is r (Fig. 2):

$$r = f\hat{\psi} - \rho = \begin{bmatrix} -p_x \\ -p_x^2/4f + f \\ 0 \end{bmatrix} = \frac{1}{4f} \begin{bmatrix} -4p_x f \\ 4f^2 - p_x^2 \\ 0 \end{bmatrix} \tag{35}$$

Dividing r by its magnitude recovers the expression in Eq. (34), confirming that the reflected ray does indeed pass through the focus.

III. Effect of Incident-Ray Perturbations on a Reflected Ray

In this section, we analyze the effect of incident-ray perturbations on reflected rays. We examine rays $\hat{r}_{\text{pert}}$ that are close enough to an exact nominal ray $\hat{r}_{\text{nom}}$ that perturbations to the rays affect them linearly (to the required accuracy). In doing this, we assumed that the ray directions are close enough to the nominal that the small-angle approximation holds. The perturbed ray direction is then

$$\hat{r}_{\text{pert}} = \hat{r}_{\text{nom}} + \mathrm{d}\hat{r} \tag{36}$$

(We make the same assumption for $\hat{i}$, $\hat{N}$, etc.) We assume that the transverse aberration (beamwalk) γ of the perturbed ray away from the nominal ray is small compared to the curvature of each element surface, so that the movement of the reflection (or refraction) point ρ is confined to a plane tangent to the surface at the nominal reflection point. We assume the motions θ and δ of the elements are small. Finally, we neglect second- and higher-order perturbations. The range of validity of these approximations is a function of the particular element type and the particular system geometry.

We represent the perturbed reflected ray in terms of its deviation from the nominal ray. The direction perturbation is $\mathrm{d}\hat{r}$, as sketched in Fig. 3. Changes in the position of the ray perpendicular to the nominal ray direction—transverse aberrations—are here termed beamwalk. Beamwalk of the reflected ray is denoted γ (Fig. 4). Changes in the length of the ray are denoted $\mathrm{d}L$. These reflected-ray perturbations are functions of the incident-ray direction perturbation $\mathrm{d}\hat{i}$, the incident-ray beamwalk α, and mirror tilt and translation perturbations θ and δ. To first order

$$\mathrm{d}\hat{r} = \frac{\partial \hat{r}}{\partial \hat{i}} \cdot \mathrm{d}\hat{i} + \frac{\partial \hat{r}}{\partial \alpha} \cdot \alpha + \frac{\partial \hat{r}}{\partial \theta} \cdot \theta + \frac{\partial \hat{r}}{\partial \delta} \cdot \delta \tag{37}$$

$$\mathrm{d}\gamma = \frac{\partial \gamma}{\partial \hat{i}} \cdot \mathrm{d}\hat{i} + \frac{\partial \gamma}{\partial \alpha} \cdot \alpha + \frac{\partial \gamma}{\partial \theta} \cdot \theta + \frac{\partial \gamma}{\partial \delta} \cdot \delta \tag{38}$$

$$\mathrm{d}L = \frac{\partial L}{\partial \hat{i}} \cdot \mathrm{d}\hat{i} + \frac{\partial L}{\alpha} \cdot \alpha + \frac{\partial L}{\partial \theta} \cdot \theta + \frac{\partial L}{\partial \delta} \cdot \delta \tag{39}$$

We derive the partial derivatives (sensitivities) of the reflected ray perturbations with respect to the incident-ray perturbations in this section. The sensitivities of the reflected ray to the mirror tilt and translation perturbations are derived in the next section. The reflected-ray direction $\mathrm{d}\hat{r}$ is sensitive to changes in the mirror normal direction, which occur when the ray incidence point moves across the surface of the (curved) mirror surface, due to incident-ray tilt, beamwalk, or mirror translation; the normal also changes when the mirror is tilted. The reflected-ray direction is also sensitive to changes in the direction of the incident ray. Reflected-ray beam walk γ is sensitive to incident-ray tilt and beamwalk.

To derive the partials of the reflected-ray direction, we differentiate the law of reflection:

$$\mathrm{d}\hat{r} = \mathrm{d}R \cdot \hat{i} + R \cdot \mathrm{d}\hat{i} \tag{40}$$

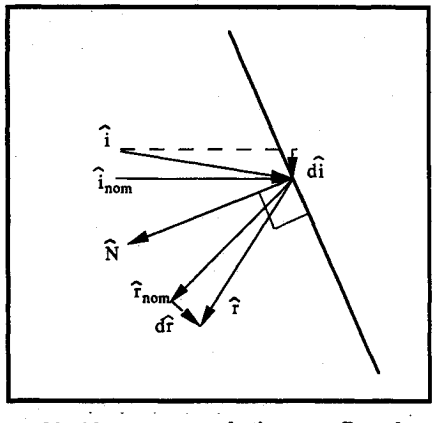

Fig. 3 Effect of incident-ray perturbation on reflected-ray direction.

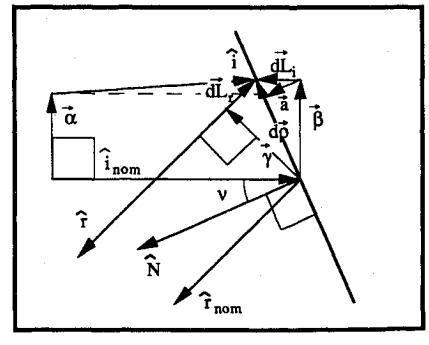

Fig. 4 Effect of incident-ray beamwalk on reflected-ray beam walk and path length.

The differential of the reflection matrix can be written in terms of deflections of the normal $\hat{N}$ as

$$dR = -2(d\hat{N}\hat{N} + \hat{N}\, d\hat{N}) \tag{41}$$

so that Eq. (36) becomes

$$d\hat{r} = \frac{\partial \hat{r}}{\partial \hat{N}} \cdot d\hat{N} + R \cdot d\hat{i} \tag{42}$$

where

$$\frac{\partial \hat{r}}{\partial \hat{N}} = -2\left[(\hat{N}\cdot\hat{i})I + \hat{N}\hat{i}\right] \tag{43}$$

As sketched in Fig. 4, the beamwalk α at the incident-ray reference point combines with the direction change $d\hat{i}$ to create the combined beamwalk β at the nominal reflection point. To first order

$$\beta = \alpha + L\, d\hat{i} \tag{44}$$

where L is the nominal path length. The perturbation in the reflection point is $d\rho$, which (Fig. 4) is

$$d\rho = \beta + dL_i \tag{45}$$

where dL_i is the incident-ray path-length change. To evaluate dL_i, consider the projection of β along the negative of the normal $(-\hat{N})$. This is denoted a, where

$$a = \hat{N}\hat{N} \cdot \beta \tag{46}$$

dL_i is the hypotenuse of the right triangle it forms with a and the tangent plane of the mirror. Denoting the angle between $\hat{i}$ and $\hat{N}$ as ν,

$$\cos\nu = -\hat{i} \cdot \hat{N} \tag{47}$$

and the change in the incident-ray path is

$$dL_i = \frac{\hat{i}\hat{N}\cdot a}{\cos\nu} = -\frac{\hat{i}\hat{N}}{\hat{i}\cdot\hat{N}} \cdot \beta \tag{48}$$

Thus, the perturbed reflection point is

$$d\rho = \left(I - \frac{\hat{i}\hat{N}}{\hat{i}\cdot\hat{N}}\right) \cdot \beta \tag{49}$$

Combining Eqs. (44) and (39), the sensitivity of the perturbed reflection point to input beamwalk is

$$\frac{\partial \rho}{\partial \alpha} = \left(I - \frac{\hat{i}\hat{N}}{\hat{i}\cdot\hat{N}}\right) \tag{50}$$

Similarly, the effect of incident-ray direction on the reflection point is

$$\frac{\partial \rho}{\partial \hat{i}} = L\left(I - \frac{\hat{i}\hat{N}}{\hat{i}\cdot\hat{N}}\right) \tag{51}$$

Recalling that the curvature of the mirror $\partial\hat{N}/\partial\rho$ is given by Eq. (21), we can now write down the effect of incident-ray direction and beamwalk on the reflected ray direction. From Eq. (42), the sensitivity of the reflected ray to incident-ray perturbations is

$$\frac{\partial \hat{r}}{\partial \hat{i}} = R + \frac{\partial \hat{r}}{\partial \hat{N}} \cdot \frac{\partial \hat{N}}{\partial \rho} \cdot \frac{\partial \rho}{\partial \hat{i}} \tag{52}$$

The sensitivity of the reflected ray to incident-ray beamwalk is

$$\frac{\partial \hat{r}}{\partial \alpha} = \frac{\partial \hat{r}}{\partial \hat{N}} \cdot \frac{\partial \hat{N}}{\partial \rho} \cdot \frac{\partial \rho}{\partial \alpha} \tag{53}$$

The effects of incident-ray direction and beamwalk on the reflected-ray beamwalk are derived easily from the geometry of Fig. 4. The reflected-ray beamwalk γ is simply the reflection of the combined incident-ray beamwalk β,

$$\gamma = R \cdot \beta \tag{54}$$

The sensitivity of the reflected-ray beamwalk to incident-ray perturbations is

$$\frac{\partial \gamma}{\partial \hat{i}} = LR \tag{55}$$

The sensitivity of the reflected-ray beamwalk to incident-ray beamwalk is

$$\frac{\partial \gamma}{\partial \alpha} = R \tag{56}$$

The effect of incident-ray perturbations on total ray path length is also derived easily from the geometry of Fig. 4. The reflected-ray path-length perturbation is the reflection of the incident-ray path-length perturbation:

$$dL_r = R \cdot dL_i \tag{57}$$

The total path-length change is the sum of these perturbations resolved along their respective rays:

$$dL = \hat{i}\cdot dL_i + \hat{r}\cdot dL_r = (\hat{i} - \hat{r}\cdot R)\cdot dL_i = 0 \tag{58}$$

Thus (to first order), incident-ray direction changes and beamwalk have no effect on the total path length:

$$\frac{\partial L}{\partial \hat{i}} = \frac{\partial L}{\partial \alpha} = 0 \tag{59}$$

IV. Effect of Mirror Perturbations on a Reflected Ray

In this section, we derive the sensitivities of the reflected ray direction $d\hat{r}$, the reflected ray beamwalk γ, and the change in path length dL to small mirror rotation θ and translation δ.

The effect of mirror translation on the reflection normal is much the same as the effect of incident-ray beamwalk: moving the mirror moves the reflection point to a region with a different normal. As the mirror moves the reflection point relative to the mirror moves opposite to it (Fig. 5):

$$d\rho = -\delta + dL_i \tag{60}$$

The path-length perturbation dL_i is derived in the same way as for the beamwalk case. The result is

$$dL_i = \frac{a}{\cos\nu} = \frac{\hat{i}\hat{N}}{\hat{i}\cdot\hat{N}} \cdot \delta \tag{61}$$

Combining Eqs. (60) and (61),

$$d\rho = \frac{\partial \rho}{\partial \delta} \cdot \delta \tag{62}$$

where

$$\frac{\partial \rho}{\partial \delta} = -\left(I - \frac{\hat{i}\hat{N}}{\hat{i}\cdot\hat{N}}\right) \tag{63}$$

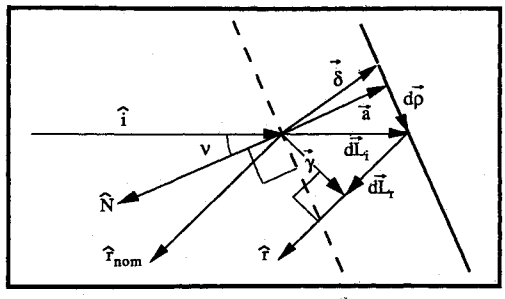

Fig. 5 Effect of mirror translation on reflected-ray beam walk and path length.

The effect of mirror translation on the reflected-ray direction is

$$\frac{\partial \hat{r}}{\partial \delta} = \frac{\partial \hat{r}}{\partial \hat{N}} \cdot \frac{\partial \hat{N}}{\partial \rho} \cdot \frac{\partial \rho}{\partial \delta} \tag{64}$$

Tilting the mirror has two effects (Fig. 6). The first is to rotate the normal. For a small mirror angle θ, the deflection in the mirror normal is

$$d\hat{N} = \theta^{\times} \cdot \hat{N} = -\hat{N}^{\times} \cdot \theta \tag{65}$$

so that

$$\frac{\partial \hat{N}}{\partial \theta} = -\hat{N}^{\times} \tag{66}$$

The second effect occurs when the center of ration is not located precisely at the point of reflection. If the vector from the rotation point to the nominal reflection point is q, then rotation will couple into translation of the nominal reflection point as

$$\delta = \theta^{\times} \cdot (p - q) = -(p - q)^{\times} \cdot \theta \tag{67}$$

so that

$$\frac{\partial \delta}{\partial \theta} = -(p - q)^{\times} \tag{68}$$

The total effect on the ray direction is

$$\frac{\partial \hat{r}}{\partial \theta} = \frac{\partial \hat{r}}{\partial \hat{N}} \cdot \frac{\partial \hat{N}}{\partial \theta} + \frac{\partial \hat{r}}{\partial \delta} \cdot \frac{\partial \delta}{\partial \theta} \tag{69}$$

A simpler alternative expression to Eq. (69) valid only for flat mirrors is given without derivation:

$$\frac{\partial \hat{r}}{\partial \theta} = -2\hat{r}^{\times} \cdot P_N \tag{70}$$

The effect of mirror translation on beamwalk can be seen in Fig. 5. It is simply the projection of dL_i perpendicular to $\hat{r}$:

$$\gamma = P_r \cdot dL_i = P_r \cdot \frac{\hat{i}\hat{N}}{\hat{i} \cdot \hat{N}} \cdot \delta \tag{71}$$

so that

$$\frac{\partial \gamma}{\partial \delta} = P_r \cdot \frac{\hat{i}\hat{N}}{\hat{i} \cdot \hat{N}} \tag{72}$$

Mirror rotation affects beamwalk only if the rotation point is not at the reflection point, so that rotation couples to translation. The effect of rotation is

$$\frac{\partial \gamma}{\partial \theta} = \frac{\partial \gamma}{\partial \delta} \cdot \frac{\partial \delta}{\partial \theta} \tag{73}$$

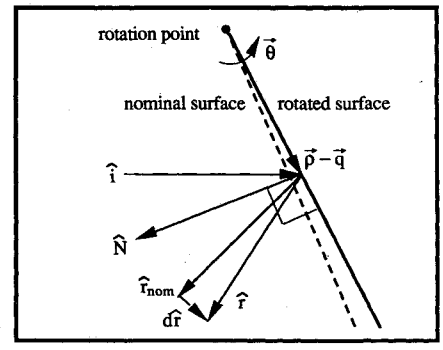

Fig. 6 Effect of mirror tilt on reflected-ray direction.

The effect of mirror translation on the path length can also be seen in Fig. 5. The total path-length change is the sum of the changes in the incident-ray and reflected-ray path lengths:

$$dL = dL_i + dL_r \tag{74}$$

The incident-ray path-length change is the magnitude of the vector dL_i:

$$dL_i = -\frac{\hat{N}}{\hat{i} \cdot \hat{N}} \cdot \delta \tag{75}$$

The reflected-ray path-length change dL_r is minus the change in the incident-ray path length projected onto the reflected ray:

$$dL_r = -(dL_i)\hat{i} \cdot \hat{r} \tag{76}$$

The path-length change due to mirror position change is:

$$dL = -\left(\frac{1 - \hat{r} \cdot \hat{i}}{\hat{i} \cdot \hat{N}}\right)\hat{N} \cdot \delta \tag{77}$$

so that

$$\frac{dL}{d\delta} = -\left(\frac{1 - \hat{r} \cdot \hat{i}}{\hat{i} \cdot \hat{N}}\right)\hat{N} \tag{78}$$

Again, mirror rotation affects path length only if the rotation point is not at the reflection point, so that rotation couples to translation. The effect of rotation is

$$\frac{\partial L}{\partial \theta} = \frac{\partial L}{\partial \delta} \cdot \frac{\partial \delta}{\partial \theta} \tag{79}$$

V. Effect of a Refracting Surface and Its Perturbations

A refracting surface is the surface bounding two regions of different index of refraction. In this section, we examine a ray passing through such a surface in the same way as we treated a ray bouncing off of a reflecting surface in the preceding sections. We assume that the shape of the surface is a conic of revolution and examine the exact effect of the surface on a general incident ray. We then derive expressions for the effects of perturbations in the incident ray and for the effects of small translation and rotation of the surface.

The refraction of a ray by a surface is governed by Snell's law (Fig. 7):

$$n_a \sin\phi_a = n_b \sin\phi_b \tag{80}$$

Here, n_a is the index of refraction of the medium containing the incident ray and n_b is the index of refraction of the medium containing the refracted ray; ϕ_a and ϕ_b are the angles of the incident ray $\hat{i}$ and refracted ray $\hat{r}$ with respect to the normal $\hat{N}$; $\hat{r}$ is in the plane defined by $\hat{N}$ and $\hat{i}$.

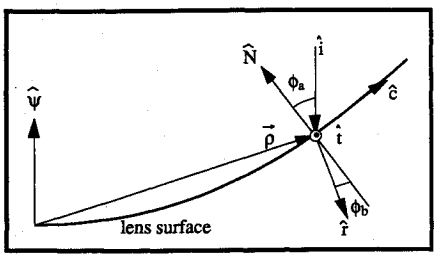

Fig. 7 Refraction geometry.

The geometry of a refracting surface is sketched in Fig. 7. Given the location p and direction $\hat{i}$ of the incident ray, and assuming that the surface is a conic of revolution (or flat), we can determine the refraction point ρ, the path length L, and the surface normal $\hat{N}$ using the equations developed in Sec. II. What remains is to find the refracted-ray direction $\hat{r}$. This we do by casting Snell's law into vector form.

Consider the vector t, where t is the cross product of the normal and incident-ray direction

$$t = \hat{N}^{\times} \cdot \hat{i} \tag{81}$$

Its magnitude is $\sin\phi_a$:

$$\sin\phi_a = \sqrt{t \cdot t} = \sqrt{-\hat{i} \cdot \hat{N}^{\times} \cdot \hat{N}^{\times} \cdot \hat{i}} \tag{82}$$

The vector c is perpendicular to both $\hat{N}$ and t, so that its magnitude is also $\sin\phi_a$:

$$c = \hat{N}^{\times} \cdot t = \hat{N}^{\times} \cdot \hat{N}^{\times} \cdot \hat{i} = -P_N \cdot \hat{i} \tag{83}$$

The refracted ray can be written in terms of its projections along the orthogonal unit vectors $\hat{c}$ and $\hat{N}$:

$$\hat{r} = -\sin\phi_b \hat{c} - \cos\phi_b \hat{N} \tag{84}$$

Writing

$$\mu = \frac{n_a}{n_b} \tag{85}$$

$-\sin\phi_b \hat{c}$ is

$$-\sin\phi_b \hat{c} = \mu P_N \cdot \hat{i} \tag{86}$$

and $\cos\phi_b$ is

$$\cos\phi_b = \sqrt{1 - \mu^2 \hat{i} P_N \cdot \hat{i}} \tag{87}$$

Substituting into Eq. (84), the refracted ray is

$$\hat{r} = \mu P_N \cdot \hat{i} - \sqrt{1 - \mu^2 \hat{i} \cdot P_N \cdot \hat{i}}\, \hat{N} \tag{88}$$

An alternate form of Eq. (88) is preferred for computational reasons:

$$\hat{r} = \mu \hat{i} - \frac{1 - \mu^2}{\sqrt{1 - \mu^2 + \mu^2 (\hat{N} \cdot \hat{i})^2} - \mu \hat{N} \cdot \hat{i}}\, \hat{N} \tag{89}$$

Equation (88) completes an exact description of the ray refracted by the surface. It starts at a point p with a direction $\hat{i}$. It travels a length L calculated from Eq. (23) and scaled by n_a as in Eq. (24). It hits the surface of the mirror at the refraction point ρ [Eq. (22)]. The normal $\hat{N}$ is calculated from Eq. (19) and the refracted-ray direction $\hat{r}$ from Eq. (89).

We now consider the effects of perturbations of the incident ray on the refracted ray. As we did for the case of a mirror, we derive the sensitivities of the refracted-ray direction $d\hat{r}$, the refracted ray transverse aberration (beamwalk) γ, and the change in path length dL to incident ray deflection $d\hat{i}$ and incident ray beamwalk α.

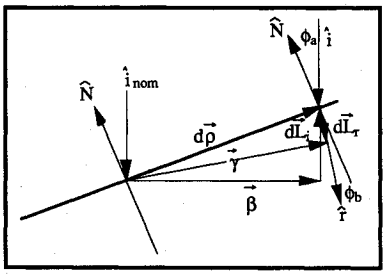

Fig. 8 Effect of incident-ray perturbations on refracted-ray beamwalk and path length.

Beamwalk affects the refracted-ray direction by moving the refraction point away from the nominal to an area of different normal. Changes in the incident-ray direction affect the refracted-ray direction by changing the angle of arrival at the refraction point as well as by causing beamwalk. The sensitivities derived in the previous sections that pertain to the surface only, such as the sensitivity of the normal to change in the refraction point $\partial\hat{N}/\partial\rho$ and the sensitivities of the refraction point to incident-ray beamwalk $\partial\rho/\partial\alpha$ and direction change $\partial\rho/\partial\hat{i}$, are the same as in the mirror case [Eqs. (50) and (51)]. The sensitivities of the refracted-ray direction to changes in the normal and to changes in the incident-ray direction are different. Differentiating Eq. (89), the effect of changes in the normal is

$$\frac{\partial\hat{r}}{\partial\hat{N}} = -\left(\frac{1 - \mu^2}{\sqrt{1 - \mu^2 + \mu^2(\hat{N} \cdot \hat{i})^2} - \mu \hat{N} \cdot \hat{i}}\right)\left(I + \frac{\mu}{\cos\phi_b} \hat{N}\hat{i}\right) \tag{90}$$

The effect of changes in the angle of arrival is

$$\left(\frac{\partial\hat{r}}{\partial\hat{i}}\right)_{\text{aoa}} = \mu\left[I + \frac{\mu}{\cos\phi_b} \hat{N}\hat{i}\right] \cdot P_N \tag{91}$$

The sensitivity of the refracted-ray direction to incident-ray beamwalk is [using Eq. (90)]

$$\frac{\partial\hat{r}}{\partial\alpha} = \frac{\partial\hat{r}}{\partial\hat{N}} \cdot \frac{\partial\hat{N}}{\partial\rho} \cdot \frac{\partial\rho}{\partial\alpha} \tag{92}$$

The effect of incident-ray direction on the refracted-ray direction is

$$\frac{\partial\hat{r}}{\partial\hat{i}} = \left(\frac{\partial\hat{r}}{\partial\hat{i}}\right)_{\text{aoa}} + \frac{\partial\hat{r}}{\partial\hat{N}} \cdot \frac{\partial\hat{N}}{\partial\rho} \cdot \frac{\partial\rho}{\partial\hat{i}} \tag{93}$$

The effect of incident-ray beamwalk on refracted-ray beamwalk γ is sketched in Fig. 8. γ is that part of ρ perpendicular to $\hat{r}$:

$$\gamma = P_r \cdot \rho \tag{94}$$

so that

$$\frac{\partial\gamma}{\partial\rho} = P_r \tag{95}$$

The sensitivity of the reflected-ray beamwalk to incident-ray beamwalk is [using Eq. (95)]

$$\frac{\partial\gamma}{\partial\alpha} = \frac{\partial\gamma}{\partial\rho} \cdot \frac{\partial\rho}{\partial\alpha} \tag{96}$$

The sensitivity of the reflected-ray beamwalk to incident-ray direction changes is

$$\frac{\partial\gamma}{\partial\hat{i}} = \frac{\partial\gamma}{\partial\rho} \cdot \frac{\partial\rho}{\partial\hat{i}} \tag{97}$$

The effect of beamwalk and incident-ray direction change on path length is also sketched in Fig. 8. The path-length change due to beamwalk (including scaling by the indices of refraction) is

$$dL = (n_a\hat{i} - n_b\hat{r}) \cdot \boldsymbol{\rho} \tag{98}$$

so that

$$\frac{\partial L}{\partial \boldsymbol{\rho}} = (n_a\hat{i} - n_b\hat{r}) \tag{99}$$

The effect of incident-ray beamwalk on the path length is

$$\frac{\partial L}{\partial \alpha} = \frac{\partial L}{\partial \boldsymbol{\rho}} \cdot \frac{\partial \boldsymbol{\rho}}{\partial \alpha} \tag{100}$$

The effect of incident-ray direction changes on the path length is

$$\frac{\partial L}{\partial \hat{i}} = \frac{\partial L}{\partial \boldsymbol{\rho}} \cdot \frac{\partial \boldsymbol{\rho}}{\partial \hat{i}} \tag{101}$$

We now consider the effect of small rotational and translational motions on the refracted ray. We derive expressions for the small changes $d\hat{r}$ in the refracted-ray direction, the refracted-ray beamwalk γ, and the change in path length dL due to surface rotation θ and translation δ.

The sensitivities of the refracted-ray direction to surface translational and rotational perturbations differ from the mirror case again only in the effect changing the normal has on the refracted-ray direction. The partials $\partial\hat{N}/\partial\boldsymbol{\rho}$, $\partial\boldsymbol{\rho}/\partial\delta$, $\partial\hat{N}/\partial\theta$, and $\partial\delta/\partial\theta$ are properties of the surface geometry. Only $\partial\hat{r}/\partial\hat{N}$ [Eq. (90)] is changed for this case. The effect of element translation on the refracted-ray direction is [using Eq. (90)]

$$\frac{\partial \hat{r}}{\partial \delta} = \frac{\partial \hat{r}}{\partial \hat{N}} \cdot \frac{\partial \hat{N}}{\partial \boldsymbol{\rho}} \cdot \frac{\partial \boldsymbol{\rho}}{\partial \delta} \tag{102}$$

The effect of surface rotation on the refracted-ray direction is

$$\frac{\partial \hat{r}}{\partial \theta} = \frac{\partial \hat{r}}{\partial \hat{N}} \cdot \frac{\partial \hat{N}}{\partial \theta} + \frac{\partial \hat{r}}{\partial \delta} \cdot \frac{\partial \delta}{\partial \theta} \tag{103}$$

The effect of translating the surface on refracted-ray beamwalk is similar to the beamwalk case, except that here the beamwalk is the projection of dL_i rather than $\boldsymbol{\rho}$ (Fig. 9). The sensitivity of γ to translation is

$$\frac{\partial \gamma}{\partial \delta} = P_r \frac{\hat{i}\hat{N}}{\hat{i} \cdot \hat{N}} \tag{104}$$

Surface rotation affects refracted-ray beamwalk only to the extent that it couples to translation,

$$\frac{\partial \gamma}{\partial \theta} = \frac{\partial \gamma}{\partial \delta} \cdot \frac{\partial \delta}{\partial \theta} \tag{105}$$

The effect of surface translation and rotation on path length is also sketched in Fig. 9. The net path-length change is

$$dL = (n_a\hat{i} - n_b\hat{r}) \cdot dL_i \tag{106}$$

The sensitivity of the path length to surface translation is

$$\frac{\partial L}{\partial \delta} = (n_a\hat{i} - n_b\hat{r}) \cdot \frac{\hat{i}\hat{N}}{\hat{i} \cdot \hat{N}} \tag{107}$$

The sensitivity of the path length to surface rotation is

$$\frac{\partial L}{\partial \theta} = \frac{\partial L}{\partial \delta} \cdot \frac{\partial \delta}{\partial \theta} \tag{108}$$

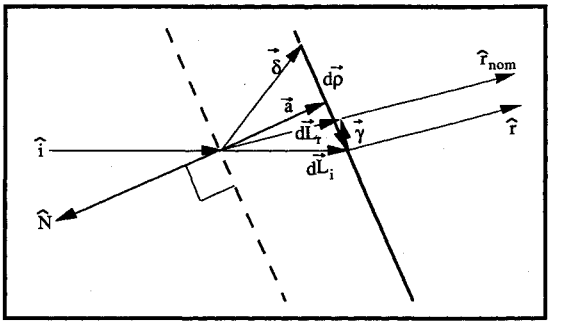

Fig. 9 Effect of surface translation on refracted-ray beamwalk and path length.

Lenses are composed of two refracting surfaces. Multiple surfaces are discussed in the next section.

VI. Multiple-Element Beam Trains

The preceding sections have derived coordinate-free expressions for tracing a ray past a single conic-of-revolution reflecting or refracting surface, given the surface eccentricity and focal length, its principal axis, the indices of refraction of the media surrounding the surface, and at the incident-ray location and direction. We also derived the sensitivities of the nominal output ray direction, transverse aberration (beamwalk), and path length to perturbations in the input ray and to small motions of the reflecting or refracting surface. The sensitivities give us a linear model of the single element for rays that are close to the exact nominal ray, as per Eqs. (37-39).

This section extends the previous results to multiple-element beam trains. We assume (without loss of generality) an element numbering scheme, numbering each element in the order that the ray strikes it, and denoting the ray segment output of each element with the subscript i. Doing this, the ray segment incident on the ith element is the ray segment output from the $i-1$ element:

$$\hat{i}_i = \hat{r}_{i-1} \tag{109}$$

$$\alpha_i = \gamma_{i-1} \tag{110}$$

The path length is accumulated:

$$L_i = \sum_{j=1}^{i} L_j \tag{111}$$

The incident-ray reference point for the subsequent element input is

$$\boldsymbol{p}_i = \boldsymbol{\rho}_{i-1} \tag{112}$$

Nominal rays are traced through the system by sequentially applying the equations of Sec. II or V while making the substitutions.

The perturbation state vector of each element can be written as $\boldsymbol{x}_i$, where

$$\boldsymbol{x}_i = \begin{bmatrix} d\hat{r}_i \\ \gamma_i \\ dL_i \end{bmatrix} \tag{113}$$

Similarly, $\boldsymbol{u}_i$ is the input vector consisting of the small translation and rotation of the ith element:

$$\boldsymbol{u}_i = \begin{bmatrix} \theta_i \\ \delta_i \end{bmatrix} \tag{114}$$

Equations (37–39) can now be written as the difference equation:

$$x_i = \frac{\partial x_i}{\partial x_{i-1}} x_{i-1} + \frac{\partial x_i}{\partial u_i} u_i \tag{115}$$

where $\partial x_i/\partial x_{i-1}$ is the transition matrix from the $i-1$th to the ith mirror,

$$\frac{\partial x_i}{\partial x_{i-1}} = \begin{bmatrix} \frac{\partial \hat{r}}{\partial \hat{i}} & \frac{\partial \hat{r}}{\partial \alpha} & 0 \\ 0 & 0 & 0 \\ \frac{\partial \gamma}{\partial \hat{i}} & \frac{\partial \gamma}{\partial \alpha} & 0 \\ 0 & 0 & 0 \\ \frac{\partial L}{\partial \hat{i}} & \frac{\partial L}{\partial \alpha} & 1 \end{bmatrix} \tag{116}$$

and $\partial x_i/\partial u_i$ is the influence matrix at the ith mirror,

$$\frac{\partial x_i}{\partial u_i} = \begin{bmatrix} \frac{\partial \hat{r}}{\partial \theta} & \frac{\partial \hat{r}}{\partial \delta} \\ \frac{\partial \gamma}{\partial \theta} & \frac{\partial \gamma}{\partial \delta} \\ \frac{\partial L}{\partial \theta} & \frac{\partial L}{\partial \delta} \end{bmatrix} \tag{117}$$

The transition and influence matrices for each surface are assembled from the optical sensitivities for that surface evaluated in the base coordinate frame and are themselves ray-state sensitivities.

The sensitivities of the ray perturbation state at one element to the state or input at another element are calculated easily as products of transition and influence matrices. The sensitivity of the state at the jth element to the state at the ith element is

$$\frac{\partial x_j}{\partial x_i} = \frac{\partial x_j}{\partial x_{j-1}} \cdots \frac{\partial x_{i+1}}{\partial x_i} \tag{118}$$

The sensitivity of the state at the jth element to the input at the ith element is

$$\frac{\partial x_j}{\partial u_i} = \frac{\partial x_j}{\partial x_{j-1}} \cdots \frac{\partial x_{i+1}}{\partial x_i} \frac{\partial x_i}{\partial u_i} \tag{119}$$

A complete linear model of a beam train combines the effects of each element as seen at the output surface. It may also include the effects of variations in the initial input ray. A line-of-sight model of the system traces a single (chief) ray through the beam train. For a system of n elements, the combined linear model of the output of a single ray through the entire beam train is the matrix C:

$$x_{n_{\text{chief ray}}} = C_{\text{LOS}} \begin{bmatrix} x_0 \\ u_1 \\ \vdots \\ u_n \end{bmatrix} = \begin{bmatrix} \frac{\partial x_n}{\partial x_0} \frac{\partial x_n}{\partial u_1} \cdots \frac{\partial x_n}{\partial u_n} \end{bmatrix}_{\text{chief ray}} \begin{bmatrix} x_0 \\ u_1 \\ \vdots \\ u_n \end{bmatrix} \tag{120}$$

A model of this sort can be useful for representing the pointing, beamwalk, and path-length behavior of a system, especially focal systems that use mainly collimated beams of light.

A wave-front model traces a number of rays distributed across the aperture. The combined ray states can be used to reconstruct the phase of the full wave front for phase plots or to interface with a physical optics function, or to calculate spot diagrams. These models take the form

$$\begin{bmatrix} x_{n_{\text{ray 1}}} \\ \vdots \\ x_{n_{\text{ray } m}} \end{bmatrix} = C_{\text{WF}} \begin{bmatrix} x_0 \\ u_1 \\ \vdots \\ u_n \end{bmatrix} = \begin{bmatrix} \begin{bmatrix} \frac{\partial x_n}{\partial x_0} \frac{\partial x_n}{\partial u_1} \cdots \frac{\partial x_n}{\partial u_n} \end{bmatrix}_{\text{ray 1}} \\ \vdots \\ \begin{bmatrix} \frac{\partial x_n}{\partial x_0} \frac{\partial x_n}{\partial u_1} \cdots \frac{\partial x_n}{\partial u_n} \end{bmatrix}_{\text{ray } m} \end{bmatrix} \begin{bmatrix} x_0 \\ u_1 \\ \vdots \\ u_n \end{bmatrix} \tag{121}$$

The reader is reminded that the absolute accuracy of the linear models is limited by the assumptions used to derive the sensitivity matrices. For systems with large motions, exact nonlinear wave-front and line-of-sight models may be preferable. Nonlinear models can also be integrated easily into standard dynamics and controls models in the form of subroutines,[7] as can subroutines to calculate optical sensitivities.

VII. Incorporating Sensors and Actuators

The joining of a linear optical model with a structural finite element or linearized multiple rigid-body model can be as simple as 1) specifying the optical system in structural coordinates, 2) referring the optical elements to particular structural nodes or bodies and choosing the rotation points q accordingly, and 3) arranging that the structural model output vector is identical to the concatenated u_i of Eqs. (120) and (121). If this is done, the joint optical and structural model is simply the matrix multiply of Eq. (120) or (121), transforming structural motion to optical system output at each update of the structure state.

Integrating the control system directly with the optical model usually requires a few additional steps. This is because the control system sensors and actuators are generally not aligned with any single coordinate system. Also, for wave-front models particularly, things affecting the sensor signals, such as diffraction effects, signal-to-noise ratios, pixel granularity, and time delays can be significant. Actuator disturbances, such as bearing noise, misalignments, and flexure hysterisis are also important dynamic effects. All of these effects can be modeled if desired. The first step in blending the control system with the optical model is, however, to incorporate the particular sensor and actuator coordinates into the optical model. We show how to do this in a couple of simple cases.

Optical sensors exist that can measure the direction of a beam of light, or its position (beamwalk), or its path length. We model these detectors by the aid of reference surfaces, by which we mean a conic of revolution or (usually) flat surface upon which the light is projected. We take reference surfaces to have no optical effect, so that $\hat{r}_{\text{RS}} = \hat{i}_{\text{RS}}$ and $\mathrm{d}\hat{r}_{\text{RS}} = \mathrm{d}\hat{i}_{\text{RS}}$. The point of incidence ρ_{RS} of a ray on the surface with respect to the vertex and its differential $\mathrm{d}\rho_{\text{RS}}$ are calculated using the relations presented previously.

As an example, a beam direction detector might be a camera or telescope located so as to sample part of a collimated beam, as in Fig. 10. For a line-of-sight optical model, such a detector can be modeled as a reference surface placed at the nominal location of the detector and oriented perpendicular to the incident ray ($\hat{\Psi}_{\text{RS}} = -\hat{i}_{\text{RS}}$). The chief ray is propagated through the beam train to the reference surface, where the ray direction $\mathrm{d}\hat{i}_{\text{RS}}$ (or $\hat{i}_{\text{RS}}$ itself for a nonlinear model) is evaluated. Neglecting second-order effects and the telescope or camera scale factor, the sensor signal is that part of $\mathrm{d}\hat{i}_{\text{RS}}$ (or $\hat{i}_{\text{RS}}$) perpendicular to $\hat{\Psi}_{\text{RS}}$. If the sensor reads out in a rectangular coordinate system, it will resolve the signal into those coordinates, $\hat{x}_{\text{RS}}$ and $\hat{y}_{\text{RS}}$, say. Assuming that the $\hat{\Psi}_{\text{RS}}$ is nominally along $\hat{z}_{\text{RS}} = \hat{x}_{\text{RS}} \times \hat{y}_{\text{RS}}$, the focal plane signal is a two vector A, where (in base coordinates)

$$A = \begin{bmatrix} \hat{x}_{\text{RS}}^T \\ \hat{y}_{\text{RS}}^T \end{bmatrix} (\hat{r} + \mathrm{d}\hat{r}) = \begin{bmatrix} \hat{x}_{\text{RS}}^T \\ \hat{y}_{\text{RS}}^T \end{bmatrix} \mathrm{d}\hat{r} \tag{122}$$

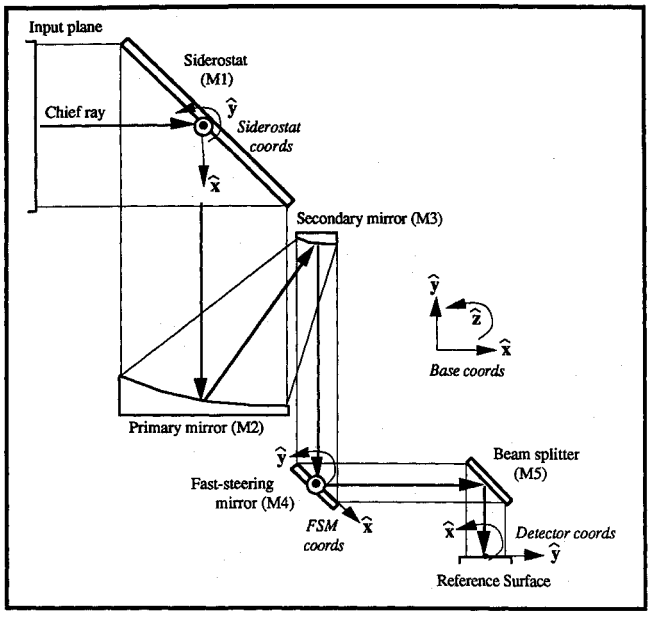

Fig. 10 Schematic of telescope example.

A can be expressed as a function of the full seven-element ray perturbation state as the 2×7 transformation T_{RS}:

$$A = T_{RS}x_{RS} = \begin{bmatrix} \hat{x}_{RS}^T & 0 & 0 & 0 & 0 \\ \hat{y}_{RS}^T & 0 & 0 & 0 & 0 \end{bmatrix} x_{RS} \tag{123}$$

The full linear model for LOS direction at the reference surface in sensor coordinates is calculated as

$$A = T_{RS}C_{LOS}\begin{bmatrix} x_0 \\ u_1 \\ \vdots \\ u_n \end{bmatrix} \tag{124}$$

For a multiple-ray wavefront model, more detailed sensor models are possible. For instance, interferometric path-length detectors measure the phase of two interfering beams of light, usually at a beam splitter. Effects that cause phase variations over the width of the beam decrease the strength of the interference signal. These effects can be captured by tracing a number of rays to a reference surface and evaluating the dL [the optical path-length difference (OPD)] of each ray. The OPD distribution can also be analyzed to decompose its defects into aberration functions, which can be useful in guiding improvements in the optical design. The OPD phase distribution together with the wave-front intensity can be converted into a complex matrix representation of the beam. This in turn can be propagated using physical optics theory to include beam diffraction effects. Point spread functions of long-distance propagation can be computed accurately in this fashion, even for relatively long wavelengths.

Wave-front spot diagrams can also be computed for wave-front models. These plots show the pierce points of each ray as it passes a reference surface. They are computed in the similar fashion to Eq. (124), except picking off γ for each ray instead of d$\hat{r}$. This sort of plot can be used to find the focus of a beam train or to simulate a wave-front or beamwalk detector. An OPD plot and spot diagram for a particular example are given in the next section.

Controller coordinates can be incorporated into the optical model in much the same way as sensor coordinates are. Typical optical control mechanisms include gimballed mirrors and gimballed telescopes, fast-steering mirrors, piston mirrors and deformable mirrors. Gimbals are single-axis rotational actuators that can be staged to provide large angular range mirror or telescope pointing capability. Fast-steering mirrors are mirrors mounted (usually) on flexure pivots to provide high bandwidth, small angular range pointing capability. Piston mirrors are actuated linearly, in the direction of the mirror normal, to provide path-length control. Deformable mirrors use a distribution of linear or other actuators behind the face of the mirror to provide control of the mirror surface figure, to correct wave-front phase.

We consider here only gimballed and fast-steering mirrors in the context of a single-ray line-of-sight model. The control coordinates are the gimbal angles taken about the gimbal bearing axes, or the fast-steering mirror actuation axes. There are typically two axes of control. For a nonredundant set of two gimbals controlling mirror tilt, we express the first actuator axis in base coordinates as $\hat{x}_m$ and at the other as $\hat{y}_m$. These axes need not be orthogonal. Then, the transformation from base to mirror coordinates is a 6×2 matrix T_m, where

$$T_m = \begin{bmatrix} \hat{x}_m & \hat{y}_m \\ 0 & 0 \\ 0 & 0 \\ 0 & 0 \end{bmatrix} \tag{125}$$

T_m is used to scale the gimbal-angle coordinates into the base coordinate frame. For element i,

$$u_i = T_m\begin{bmatrix} \theta_x \\ \theta_y \end{bmatrix} \tag{126}$$

Other types of actuators can be handled as simply. Note that the components of T_m need not be unit vectors. Translational actuators tend to couple into element rotation, producing element tilts proportional to the distance from the center of rotation.

The integration of sensor and actuator coordinates into the optical model is particularly useful for the determination of optical gains of controlled elements in an invertable form. Consider a beam train with n elements, the first of which is a gimballed mirror and the last of which is a direction detector (numbered from 2 to n) between a steering mirror m and a focal plane. The mirror is to be controlled to center the line of sight on the reference surface. First, let us determine the optical gain of the mirror, which is simply the sensitivity of the detector tilt signal to the gimbal actuator angles. The sensitivity of the chief-ray perturbation state at the reference surface to element inputs is determined following the analysis presented in the previous sections as $\partial x_n/\partial u_1$. The optical gain is this matrix scaled by the sensor and actuator coordinate transformations derived earlier (here $\theta_m = [\theta_x \theta_y]^T$):

$$\frac{\partial A}{\partial \theta_m} = T_{RS}\frac{\partial x_n}{\partial u_1}T_m \tag{127}$$

This expression, being a 2×2 matrix of rank 2, is invertible. The result,

$$\frac{\partial \theta_m}{\partial A} = \left[\frac{\partial A}{\partial \theta_m}\right]^{-1} \tag{128}$$

is the transformation of the detector tilt signal to the gimbal actuator angles. The two vector of mirror angles θ_m that produce a focal plane signal of A is, thus,

$$\theta_m = \frac{\partial \theta_m}{\partial A}A \tag{129}$$

Table 1 Optical parameters for beam-compressor telescope example

Surface	Location (x,y cm)	Normal at chief ray	Notes
M1	(−120, 167)	(−0.707, −0.707,0)	Flat siderostat with two large-angle gimbals
M2	(−87, 167)	(0.991, 0.131, 0)	Primary mirror for collector: $f=116.33$, $e=1$
M3	(−60, 130)	(−0.991, −0.131, 0)	Collector secondary: $f=14.54$, $e=1$
M4	(−60, 20)	(0.707, 0.707, 0)	Flat fast-steering mirror with two small-angle articulation axes
M5	(0, 20)	(−0.707, −0.707, 0)	Flat beam splitter
RS	(0, 0)	(0, 1, 0)	Photon camera focal plane

Table 2 C-matrix for beam-compressor telescope example

Partial of LOS at reference surface to ray at element 0 (input ray)							
	$d\hat{r}_x$	$d\hat{r}_y$	$d\hat{r}_z$	γ_x	γ_y	γ_z	dL
$d\hat{r}_x$	−0.2384E−06	−0.8000E+01	0.0000E+00	−0.3183E−24	−0.2328E−08	0.0000E+00	0.0000E+00
$d\hat{r}_z$	0.0000E+00	0.0000E+00	0.8000E+01	0.0000E+00	0.0000E+00	0.0000E+00	0.0000E+00
Partial of LOS at reference surface to siderostat (M1) perturbations							
	θ_x	θ_y	θ_z	δ_x	δ_y	δ_z	
$d\hat{r}_x$	0.0000E+00	0.0000E+00	0.1600E+02	0.2328E−08	0.2328E−08	0.0000E+00	
$d\hat{r}_z$	−0.8000E+01	0.8000E+01	0.0000E+00	0.0000E+00	0.0000E+00	0.0000E+00	
Partial of LOS at reference surface to primary mirror (M2) perturbations							
	θ_x	θ_y	θ_z	δ_x	δ_y	δ_z	
$d\hat{r}_x$	0.0000E+00	0.0000E+00	−0.1600E+02	0.6524E−01	−0.1762E−01	0.0000E+00	
$d\hat{r}_z$	0.1572E+02	−0.2085E+01	0.0000E+00	0.0000E+00	0.0000E+00	0.6758E−01	
Partial of LOS at reference surface to secondary mirror (M3) perturbations							
	θ_x	θ_y	θ_z	δ_x	δ_y	δ_z	
$d\hat{r}_x$	0.0000E+00	0.0000E+00	0.2000E+01	−0.6524E−01	0.1762E−01	0.0000E+00	
$d\hat{r}_z$	−0.1965E+01	0.2607E+00	0.0000E+00	0.0000E+00	0.0000E+00	−0.6758E−01	
Partial of LOS at reference surface to FSM (M4) perturbations							
	θ_x	θ_y	θ_z	δ_x	δ_y	δ_z	
$d\hat{r}_x$	0.0000E+00	0.0000E+00	−0.2000E+01	0.0000E+00	0.0000E+00	0.0000E+00	
$d\hat{r}_z$	0.1000E+01	−0.1000E+01	0.0000E+00	0.0000E+00	0.0000E+00	0.0000E+00	
Partial of LOS at reference surface to beam splitter (M5) perturbations							
	θ_x	θ_y	θ_z	δ_x	δ_y	δ_z	
$d\hat{r}_x$	0.0000E+00	0.0000E+00	0.2000E+01	0.0000E+00	0.0000E+00	0.0000E+00	
$d\hat{r}_z$	−0.1000E+01	0.1000E+01	0.0000E+00	0.0000E+00	0.0000E+00	0.0000E+00	

VIII. Example

To illustrate the application of our approach, we analyze a simple off-axis afocal telescope system. This is sketched in Fig. 10; key parameters are summarized in Table 1. Our example is a simplification of part of the Focus Mission Interferometer (FMI), a proposed space-based long-baseline stellar imaging and astrometry instrument.[1]

As shown, the first mirror the starlight sees is a flat siderostat mirror, which is actuated in two axes: a clock gimbal fixed between the base structure and an intermediate structure and a cone gimbal fixed between the intermediate structure and the mirror backplane. The mirror is steerable over large angles at low bandwidth. The siderostat directs the starlight toward mirrors 2 and 3, which form an off-axis afocal beam compressor telescope consisting of two confocal parabolic mirrors. Mirror 4 is a fast-steering mirror (FSM), steerable over small angles at high bandwidth. For this example, we have interposed a beam-splitter, at which interference with light from a similar telescope at the other end of the baseline takes place, and a direction detector to measure tilt angles. The FSM controller senses ray angle at the detector, driving the FSM to stabilize the line of sight at high bandwidth. The siderostat controller provides follow-up control to the FSM, sensing FSM angle and moving at low bandwidth to drive it to null. The science figure of merit is the wave-front phase and tilt as measured at the beam splitter.

A linear line-of-sight C_{LOS} model was computed with the siderostat fixed as shown in Fig. 10. Taking the detector axes as shown ($\hat{x}_{RS}=\hat{z}$, $\hat{y}_{RS}=\hat{x}$), we recast the C_{LOS} model into detector coordinates. The resulting model computes two axes of ray direction, as summarized in Table 2. The magnification of input-ray perturbations as seen at the detector is 8 times. The sensitivity of the detector tilt signal to either siderostat or primary mirror tilt is 16 times about the base $\hat{z}$ axis; other components depend on mirror orientation. Sensitivity to perturbations of elements in the reduced-aperture part of the beam train is more like 2 times in their sensitive axes.

The optical gains of the FSM are nearly constant, as the FSM has a very limited angular range. The actuator coordinate transformation in base coordinates is determined from inspection of Fig. 10 as

$$T_{FSM}=\begin{bmatrix} 0.707 & 0 \\ -0.707 & 0 \\ 0 & 1 \\ 0 & 0 \\ 0 & 0 \\ 0 & 0 \end{bmatrix} \tag{130}$$

The optical gain [Eq. (127)] of the FSM is thus

$$\frac{\partial A}{\partial \theta_m}=\begin{bmatrix} 0 & -2 \\ 1.414 & 0 \end{bmatrix} \tag{131}$$

The transformation from the detector signals to actuator angles is the inverse of this [Eq. (129)]

$$\frac{\partial \theta_m}{\partial A}=\begin{bmatrix} 0 & 0.707 \\ -0.5 & 0 \end{bmatrix} \tag{132}$$

The optical gains of the siderostat are a function of the gimbal angles. The clock axis is fixed in base coordinates as $\hat{x}_{sid}=[0 \quad -1 \quad 0]^T$. The cone axis varies in base coordinates as a function of θ_x: $\hat{y}_{sid}=[\cos\theta_x \quad 0 \quad \sin\theta_x]^T$. The mirror normal is a function of both gimbal angles:

$$\hat{N}_{sid}=\left[-\sin\theta_x \cos\theta_y \quad -\sin\theta_y \quad \cos\theta_x \cos\theta_y\right]^T \tag{133}$$

The initial attitude of the mirror aligns the normal with the base $\hat{z}$ axis. The partial of the detector tilt with respect to the mirror angle for a flat mirror in detector coordinates, as a

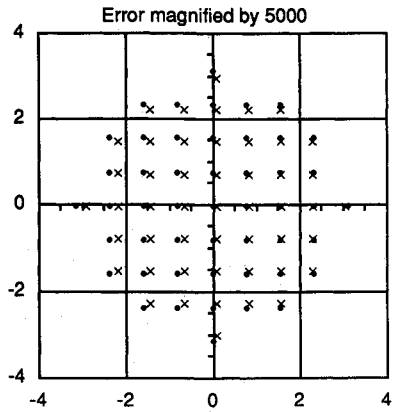

Fig. 11 Spot diagram for telescope example.

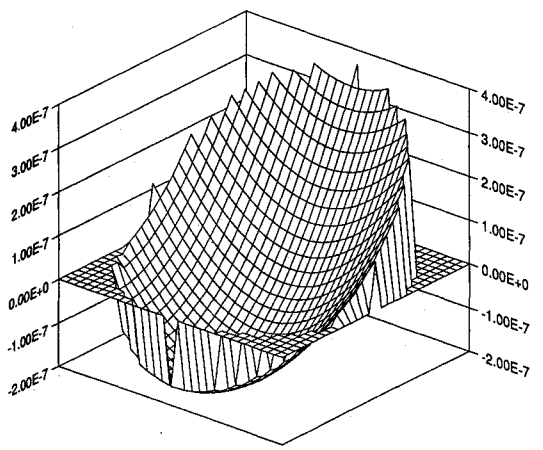

Fig. 12 Optical path-length difference distribution for telescope example.

function of the siderostat gimbal axes is, from Eq. (73),

$$\frac{\partial A}{\partial \theta} = -2\frac{\partial \hat{r}_{RS}}{\partial \hat{r}_1}\begin{bmatrix}1 & 0 & 0\\ 0 & 0 & 1\end{bmatrix}\hat{r}^{\times}(I-\hat{N}\hat{N}^T) = \begin{bmatrix}0 & \cos\theta_x\\ -1 & 0\\ 0 & \sin\theta_x\end{bmatrix} \tag{134}$$

Substituting for $\hat{N}$ from Eq. (133), using $\hat{r}=[0 \quad -1 \quad 0]^T$, and calculating the telescope gain without the siderostat as

$$\frac{\partial \hat{r}_{RS}}{\partial \hat{r}_1} = \begin{bmatrix}8 & 0 & 0\\ 0 & 0 & 0\\ 0 & 0 & 8\end{bmatrix} \tag{135}$$

the optical gains [Eq. (134)] reduce to

$$\frac{\partial A}{\partial \theta_{sid}} = -16\begin{bmatrix}\cos\theta_x \sin\theta_y \cos\theta_y & -\sin\theta_x\\ \sin\theta_x \sin\theta_y \cos\theta_y & \cos\theta_x\end{bmatrix} \tag{136}$$

As for the FSM, this expression can be inverted to compute the transformation from detected tilt to gimbal angles. The transformation from siderostat angles to FSM angles is the product of this transformation and the optical gains of the FSM.

A particular perturbation case was computed using a wave-front model to show the varying response of rays across the aperture to beam-train perturbations. The perturbation is a 10-μm translation of the telescope primary mirror in the direction of the normal at the chief ray incidence point (Table 1). The spot diagram of Fig. 11 shows 49 ray pierce points at the reference surface. The nominal unperturbed pierce points are indicated by solid dots and the perturbed pierce points by $\times$. The spread pattern shows primarily defocus aberration. The OPD distribution of Fig. 12 shows wave-front phase in meters for 709 rays (a common piston component of 19.8 μm was subtracted out). Again, the plot shows defocus aberration.

IX. Conclusions

We have presented a systematic mathematical approach to the modeling of optical beam trains for the purposes of integrated structure, controls, and optics analysis. Beyond providing specific results, we have shown a general method that can be extended to include other optical elements, other types of perturbations, and other representations of optical performance. Incorporating any optical element whose surface and optical effects can be expressed analytically follows the example developed here for reflecting and refracting surfaces. Modeling of multiple paths through a beam train for multiple-aperture or segmented telescopes is straightforward. Perturbations of parameters such as element focal length, eccentricity, or index of refraction are easily derived: these are useful for optical design optimization. Physical optics analysis functions can be incorporated. These extensions have been realized in a general optical model-generation computer code, which will be reported on in a separate paper.

Acknowledgment

This research was performed at the Jet Propulsion Laboratory, California Institute of Technology, under contract with NASA.

References

[1]Laskin, R., and San Martin, M., "Control/Structure Design of a Spaceborne Optical Interferometer," American Astronautical Society, Paper 89-424, Aug. 1989.

[2]Redding, D., Chien, T., Kopf, E., and Wong, E., "Space-Stabilized Beam Pointing for a Bifocal Satellite Experiment," American Astronautical Society, Paper 89-032, Feb. 1989.

[3]Morine, L., "Zenith Star: A Controls Challenge," American Astronautical Society, Paper 89-037, Feb. 1989.

[4]Shao, M., et al., "The Mark III Stellar Interferometer," *Astronomy and Astrophysics,* Vol. 193, 1988.

[5]Laskin, R., Breckenridge, W., Shao, M., and Redding, D., "Calibration and Operation of a Large Space-Based Optical Interferometer," American Astronautical Society, Paper 90-040, Feb. 1990.

[6]Rodden, J., "Mirror Line of Sight on a Moving Base," American Astronautical Society, Paper 89-030, Feb. 1989.

[7]Breckenridge, W., and Redding, D., "Preliminary SRE Acquisition Error Analysis," Jet Propulsion Lab., Pasadena, CA, Engineering Memo 343-1030, Aug. 1986.

[8]Wette, M., Milman, M., and Redding, D., "Experiences in Integrated Structure/Optics/Control Design Optimization," *Proceedings of the Fourth NASA/DOD Control Structure Interaction Technology Conference,* Wright Lab., Eglin AFB, FL, Jan. 1991.

[9]Silberstein, L., *Simplified Method of Tracing Rays Through Any Optical System,* Longmans, Green, London, 1918.